Evaluating Postharvest Washing Methods for Micro-Nanoplastic Removal from Edible Vegetable Leaves

Mingjiu Liu[1,2], Anupam Das[1], Lynn R. Terry[1], Huiyuan Guo*[1,2]

1 Department of Chemistry, State University of New York at Binghamton, Binghamton, NY, 13902, USA

2 Department of Material Science and Engineering, State University of New York at Binghamton, Binghamton, NY, 13902, USA

*Corresponding Author: Guo, Huiyuan (hguo@binghamton.edu)

Abstract

Micro and nano-plastics (MNPs) have become a significant contamination concern in various ecosystems. In agriculture, they contaminate edible plants through different sources, such as irrigation and air deposition, threatening food safety and human health. It is uncertain whether post-harvest cleaning methods can effectively remove MNPs from the surface of edible plants. This study used confocal Raman spectroscopy and surface-enhanced Raman spectroscopy (SERS) to assess the efficacy of household and industrial postharvest washing methods in removing MNPs from vegetable leaf surfaces. In particular, the cleaning techniques included tap water washing, vegetable detergent washing, and sonication cleaning. The plastic particles tested included 42 μm polystyrene (PS), 6 μm polymethyl methacrylate (PMMA), and 61 nm PS. In evaluating cleaning methods to remove MNPs from basil leaves, the tap water washing method demonstrated high removal efficacy for 42 μm PS (93.1%) but lower efficacy for 6 μm PMMA (51.6%). Vegetable detergent was the most effective method for PMMA removal (73.3%). The sonication method exhibited the highest removal efficacy of 59.8% among the three washing methods for removing 61 nm PS. This is the first time that the efficacies of common washing methods to remove MNPs from fresh produce were evaluated and compared using confocal Raman spectroscopy and SERS. The research offers critical insights and approaches for assessing the removal efficacy of commonly used washing techniques in decontaminating MNPs from fresh produce. The findings highlight the need to develop more effective washing methods to enhance MNPs removal in the future.

Keywords: SERS, removal efficacy, polystyrene nanoplastics, in-situ confocal Raman imaging, plastic contamination

Graphical Abstract

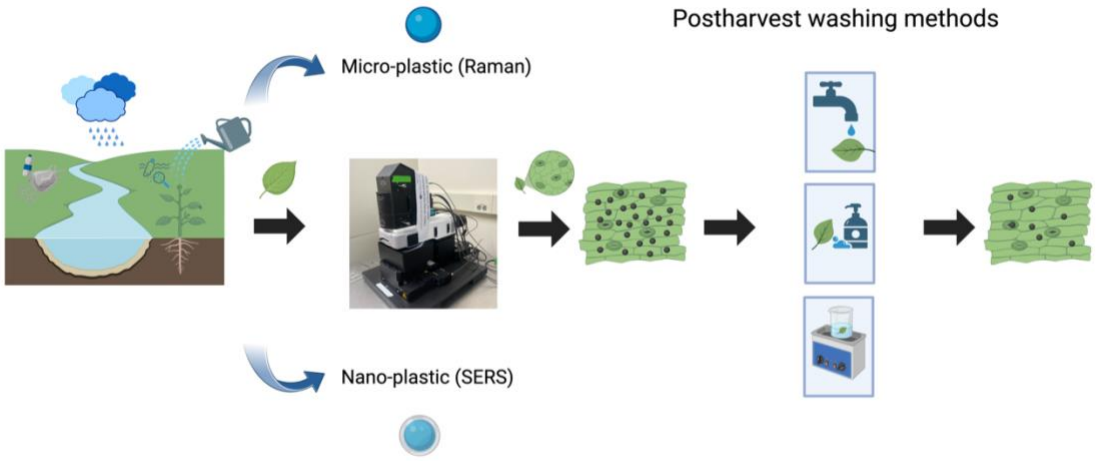

Created with BioRender.com

1. Introduction

Plastics have found wide applications in various aspects of our lives.[1,2] Because of the high utilization of plastics and its low recycling rates,[3] plastic contamination impacts a wide range of ecosystems, such as agricultural[4] and aquatic environments.[5] Larger plastic debris in the environment will undergo degradation, breaking down into smaller fragments,[6] due to various environmental factors, such as UV radiation,[7] mechanical abrasion,[8] and chemical weathering.[9] The smaller pieces may be invisible to the naked eye, accumulating without being noticed. The presence of plastic debris, often classified as microplastics (MPs, measuring 1 μm-5 mm) and nanoplastics (NPs, measuring less than 1 μm),[10] has led to adverse impacts on both human health and the environment.[11] Microplastics and nanoplastics (MNPs) can easily contaminate and transport in freshwater ecosystems (e.g.streams, ponds, lakes, rivers, and dams)[12] through wind transport,[13] atmospheric depositions,[14] and surface runoff from nearby lands.[15] MNPs enter agricultural lands through multiple pathways, such as plastic mulch application,[16] sewage sludge,[17] and irrigation.[18] Those processes were reported to result in annual input of 63,000–430,000 tons of MNPs in European farmlands per year, 44,000-300,000 tons in North American agricultural landscapes, and 2,800-19,000 tons in Australian agricultural lands.[19]

There are concerns about the contamination of crops by MNPs-containing irrigation water, causing food safety and potential health risks. Research conducted in Taiwan examined irrigation water collected around the world and found the presence of MPs in all water samples.[20] Another recent study conducted in Italy investigated the quantity of MPs present in vegetables purchased from local markets. The highest concentration of MPs was detected ranging from 72,175 to 130,500 particles/gram in sampled vegetables.[21] Edible plants like crops can be exposed to MNPs from irrigation water through foliar contact. Recent studies have revealed that foliar MNP exposure

harmed plant growth and health, as MNPs adhered to plant leaves, they accumulated and underwent translocation within the plants.[22–24] Therefore, it is crucial to control or eliminate crop contamination by MNPs and reduce human exposure and risk. Several household postharvest washing methods are commonly used to remove soil, dirt, and environmental pollutants from vegetable leaves,[25] such as rinsing with tap water and soaking in food detergent. Besides household washing methods, industrial postharvest washing techniques for cleaning vegetables may also be applied to ensure the cleanness and quality of vegetables before packaging.[26] Sonication is one of the most common industrial washing methods to eliminate large visible contaminants.[27,28] While these methods can remove certain contaminants and pathogens,[25–28] their ability to clean MNPs off vegetable leaves remains unknown.

To the best of our knowledge, there has been limited investigation evaluating the efficacy of postharvest washing methods to remove MNPs from leafy vegetable surfaces. Failure to address this question will jeopardize food safety, as foliar MNP contamination on edible plants can adversely affect human health. Recent studies have proven MNPs as a potential contributing factor to autism spectrum disorder, as well as a potential trigger for myocardial infarction, stroke, and even death among patients with detected MNPs in carotid artery plaque.[29,30] However, owing to the extremely small size of NPs, there is a shortage of reliable approaches to detect NPs. Direct detection of NPs in/on biological matrices without any labeling is difficult, even with the assistance of an optical microscope. Electron microscope-based techniques, such as Transmission Electron Microscope (TEM) and Scanning Electron Microscope (SEM) coupled with Energy Dispersive X-ray Spectroscopy (EDX), are frequently used for NP characterization. Nevertheless, the sample preparation and analysis are time-consuming and expertise-demanding.[31] Confocal laser scanning microscopy (CLSM) and fluorescence microscopy (FM) have been used to detect and monitor

fluorescent dye-labeled NPs (FNPs) within biological structures.[32,33] However, they rely on the use of fluorescent dyes, and the results are flawed by multiple artifacts and weaknesses: 1) false positive results and potential toxicity to the tested organisms due to the leakage of fluorescent dyes from the NPs;[34–36] 2) low signal stability induced by photobleaching;[37] 3) analytical interference by biological autofluorescence.[32,38]

To address the above knowledge gaps and technical challenges, the objective of this study is to use confocal Raman spectroscopy to evaluate the efficacy of different postharvest washing methods to remove MNPs from vegetable leaves. We examined two common types of plastic particles found in the environment.[39] Specifically, we chose polystyrene (PS) particles with sizes of 42 µm and 61 nm, and polymethyl methacrylate (PMMA) particles with a size of 6 µm. We selected three washing methods for our study: rinsing with tap water, soaking in vegetable detergent followed by rinsing with tap water, and sonication. These methods were chosen because they are commonly used in household or industrial settings for washing vegetables. To assess the efficacy of these methods in removing MNPs from vegetable leaves, we used confocal Raman spectroscopy imaging to detect the MNPs on leaves before and after washing. To tackle the challenge of detecting NP in biological samples, we developed a novel NP model that allows in-situ assessment of NP removal by confocal surface-enhanced Raman spectroscopy (SERS). Evaluating existing postharvest washing methods will help us predict MNP residues on fresh produce and potential human ingestion. Further, the results will guide the development of new practices and strategies to reduce MNP exposure. Our research findings have the potential to improve consumer awareness and industry regulation of MNP contaminations, contributing to a cleaner, safer, and more sustainable food chain.

2. Materials and methods

2.1 Materials

Sodium citrate dihydrate and ascorbic acid were purchased from Fisher Chemical. Gold acid chloride trihydrate ($HAuCl_4 \cdot 3H_2O$) with a purity of ≥99.9% trace metals basis was obtained from Sigma Aldrich. Hydrochloric acid (HCl) was purchased from Fisher Chemical, while sodium hydroxide (NaOH) was acquired from Sigma Aldrich. 4-Mercaptobenzoic acid (4-MBA) was obtained with a purity of 90% from Sigma Aldrich. Polyvinylpyrrolidone (PVP) with an average molecular weight of 10,000 was sourced from Sigma Aldrich. Divinylbenzene (DVB) with a purity of 80% was purchased from Sigma Aldrich. Styrene (ST), which contains 4-tert-butylcatechol as a stabilizer and has a purity of ≥99.9% was sourced from Sigma Aldrich. Additionally, 1.7 wt.% 2-methyl-propionamidine dihydrochloride (AIBA) with a purity of 97% was obtained from Sigma Aldrich.

2.2 Preparation of MNPs

PS and PMMA spherical MPs were purchased from Polyscience Inc., with an average diameter of 42 µm and 6 µm, respectively. The model NP exhibits a core-shell structure, wherein the 4-MBA-labeled gold core serves as the SERS nanotag, and the PS shell simulates the plastic surface. To synthesize the gold nanoparticles (nAu), citrate-stabilized gold seeds were first prepared by adding 1.0 mL of 1.0 wt.% sodium citrate to 100 mL of boiling 0.001 wt.% $HAuCl_4 \cdot 3H_2O$ with stirring and refluxing. The mixture was maintained at a boil for 30 minutes and then allowed to cool down to room temperature; this was used as the citrate-stabilized gold seed suspension. Subsequently, 100 µL of the citrate-stabilized gold seed suspension was added to 10 mL of 1 mM HCl and 50 µL of 50 mM $HAuCl_4 \cdot 3H_2O$ solution under stirring at 700 rpm. To this mixture, 50 µL of freshly prepared 100 mM ascorbic acid was added while stirring at the same speed for 30 seconds. The

suspension was then centrifuged for 15 minutes at 4500 rpm, and the supernatant was discarded while retaining the precipitate. This process was repeated for 4 more times and the nAu were combined and resuspended to a final volume of 5 mL in ultrapure water; nAu were stored in a refrigerator (4 ℃) for further use.

To enable SERS imaging, the nAu surface was labeled with a Raman indicator, 4-MBA. This indicator was chosen because of its sharp, characteristic SERS peaks, as well as covalent bonding with nAu through the Au-S bond that prevents leakage of 4-MBA. To label the nAu core, 7 µL of 100 mM NaOH was added to a 3.5 mL nAu suspension synthesized above and incubated for 10 minutes to prevent aggregation. Subsequently, 35 µL of 10 mM 4-MBA in ethanol was added to the nAu suspension and incubated for 10 minutes. The 4-MBA-labeled nAu were then subjected to centrifugation for 30 minutes at 4500 rpm to eliminate excess 4-MBA molecules. The supernatant was discarded, and the particles were resuspended in 3.5 mL of ultrapure water.

The labeled nAu were used to make the core-shell structure by growing a PS polymer layer on the surface. In a 150 mL three-neck round bottom flask equipped with a thermometer and a reflux condenser, 0.15 g of PVP was added to a mixture of 40.25 mL of ethanol and 9.75 mL of ultrapure water. While stirring at 1000 rpm, 25 µL of DVB and 475 µL of ST were added. The reaction proceeded under nitrogen for one hour at 70 ℃. Subsequently, 1.5 mL of 1.7 wt.% AIBA was added to the flask and stirred for 8 minutes. Following this, 3.5 mL of 4-MBA-labeled nAu were added to the flask and allowed to react for one hour. The PS NP suspension was then centrifuged three times with ultrapure water for 10 minutes at 10,000 rpm to remove excess reactants. Finally, the PS NPs were diluted to 1.2×10^9 particles/µL in a volume of 0.5 mL with ultrapure water. The synthesized model PS NPs were characterized by Dynamic Light Scattering (DLS, Zetasizer Nano

ZS, Malvern Instruments), TEM (JEOL JEM 2100F), and Ultraviolet-Visible spectroscopy (UV-Vis, HP/Agilent 8453).

2.3 Basil plant cultivation and MNP exposure

Fresh basil plants were purchased from a local grocery store (Binghamton, NY, USA). The basil plants were placed inside a clean chamber to ensure optimal exposure to light and a well-regulated airflow. This environment was designed to simulate conditions conducive to the plant's growth and development, providing a controlled setting for experiments. In the process of leaf selection for our experiments, the choice was made to choose face-up leaves. It was guided by the likelihood of these leaves encountering MNPs during agricultural irrigation. Additionally, we maintained consistency in leaf size by selecting leaves of similar size for each experiment. Before MNP exposure, the leaf surface was gently cleaned with ultrapure water and examined by confocal Raman spectroscope to ensure no MNP contamination. The basil leaves were treated with PS MPs, PMMA MPs, and PS NPs at concentrations of 5.01 µg/g of leaf, 10.19 µg/g of leaf, and 0.054 µg/g of leaf, respectively. A prior study has found the highest concentration of MPs in edible fruits and vegetables to be 13.82 µg/g.[21] Therefore, the MNP concentrations we used are within the vegetable exposure range.

2.4 Postharvest washing methods

We evaluated postharvest washing techniques to determine their efficacy in removing MNPs from the basil leaf surface. We specifically studied the impact of three commonly used household methods: tap water rinsing, vegetable detergent washing, and sonication. To ensure the reliability of results, three replicates were prepared in each group.

2.4.1 Tap water washing

The MNPs-contaminated basil leaf was placed under a running tap, and water was allowed to flow vertically, directly onto the contaminated area. Care was taken to ensure that the entire contaminated area surface received a thorough flush without excessive splashing, maintaining a moderate flow. This flushing process was continued for 30 seconds. Following that, the basil leaf was left to air dry.

2.4.2 Vegetable detergent washing

The vegetable detergent was purchased from a local supermarket. It was applied based on the user guide by spraying five times onto the MNP-contaminated area of a basil leaf. The spray was allowed to soak the contaminated area for 5 minutes. Subsequently, the basil leaf went through the previously described tap water rinsing procedure for 30 seconds. Following the rinsing process, the leaf was left to dry.

2.4.3 Sonication

For the sonication method, a Branson ultrasonic bath model 8800 was used to remove MNPs from basil plant leaves. The ultrasonic bath operated at a frequency of 40 kHz, and the procedure was conducted at room temperature (~25 °C). In a 50 mL beaker, 40 mL of ultrapure water was added. The basil leaf was immersed in the beaker and subjected to sonication for 1 minute. Subsequently, the leaf was carefully removed from the beaker and allowed to dry.

2.5 Confocal Raman Microscopy Imaging

We used the Alpha300R advanced Raman spectroscope (WITec), featuring a 785 nm laser. This advanced instrument is integrated with a confocal microscope, offering magnification options of 10x, 50x, and 100x. Equipped with an automated scanning system, this instrument facilitates 2D SERS imaging. This capability is made possible through a motorized X-Y sample scanning stage

and Z-focusing function. Consequently, it allowed us to generate both bright-field images and Raman maps of the MNPs on basil leaves. To ensure the quality of Raman imaging, we optimized the instrumentation settings before detection, such as the laser power of confocal Raman, integration time, and scanning step size. The collected data were processed using Project Five+ to correct the spectra, extract relevant characteristic Raman peaks from spectra, and generate Raman signal maps of MNPs. By utilizing this technique before and after washing, we could assess the efficacy of each postharvest washing method in removing MNPs from basil leaves.

2.6 Postharvest washing methods efficacy quantification by ICP-MS

In addition to confocal Raman imaging, ICP-MS was used to better accurately quantify the efficacy of these postharvest washing methods in removing model NP from basil leaves. The model NP required acid digestion before ICP-MS due to its structure, which consists of a PS shell surrounding a gold core. The initial step in ICP-MS sample preparation involved sonicating the model NP particles with basil leaves for 5 minutes to break down the PS shell. To digest the gold core of the model NP for ICP-MS detection of the gold element, we digested them with 1 mL of aqua regia at room temperature for 2 hours. Lastly, the digested samples were filtered using Biomed Scientific's Nylon Syringe Filters, which have a 25 mm diameter and a pore size of 0.45 µm and diluted to the desired concentrations for ICP-MS analysis. To ensure the gold concentration was sufficiently high for detection by ICP-MS, we applied 10 1 µL droplets of 0.054 µg/g of model NP on basil leaves, which is significantly more than what was used for confocal Raman imaging. To compare the washing efficacies in removing model NP from basil leaves, four groups of samples were prepared: model NP on basil leaves before washing, model NP on basil leaves after washing with tap water, model NP on basil leaves after washing with detergent, and model NP on basil leaves after sonication. Each group included three replicates to ensure accuracy.

3. Results and discussion

In this project, three postharvest washing methods were used to remove MNPs from basil leaves. The results aim to determine whether the applied methods are effective for MNP removal and, if not, to identify the most effective washing approach among the techniques. We used two types of MPs - PS (42 µm) and PMMA (6 µm), and one type of NP - model PS (61 nm) to evaluate the efficacy of different washing techniques in removing MNPs from vegetable leaves. To begin the experiment, we applied 0.5~1.0 µL droplet of each type of plastic particle suspension onto basil leaves. Microscopic images were taken before and after washing to visually observe the difference in MNP presence. Additionally, Raman surface area scans were conducted to generate Raman maps before and after washing to track the removal of MNPs. The three washing methods were 30-second tap water flushing; immersion in vegetable detergent for 5 minutes followed by a 30-second tap water flush; and a 1-minute sonication in a beaker. Tap water rinsing is a common routine practice in most households, while vegetable detergent washing is often used in either household or commercial facilities for cleaning produce. Sonication technique involves the use of high-frequency ultrasound waves to dislodge particles from vegetable surfaces and is a method with potential advantages in small particle removal. Assessing these common methods will advance our understanding of their cleaning efficacy and offer valuable insights for pollutant removal method development in the future. The PS MPs and PMMA MPs were purchased from the manufacturer. To confirm their sizes, we captured their microscopic images, and measured the sizes with ImageJ, obtaining an average size of 42 $\pm$ 0.23 µm for PS MPs and 6 $\pm$ 1.3 µm for PMMA MPs (**Fig. S1**).

3.1 MNP characterization

To evaluate the removal of NPs by different washing methods, we developed a novel NP model that allows multi-dimensional imaging of NPs by SERS. The model NPs consist of Raman indicator-labeled nAu (also called SERS nanotags) as the core and a plastic layer as the shell that simulates the target plastic surface. The nAu core enhances Raman indicator signals so that model NPs can be tracked directly by SERS. SERS is an advanced technique that integrates normal Raman spectroscopy with nanotechnology. Unlike conventional Raman spectroscopy, SERS achieves higher sensitivity through the integration of noble metal nanoparticles, significantly increasing Raman signals by orders of magnitude (10^5~10^{10}).[40] SERS has several unique advantages for imaging NPs in biological systems: 1) it has high stability and is not affected by photobleaching or biological autofluorescence in contrast to fluorescence-based methods; 2) Raman bands are narrower than fluorescence bands, providing molecular information with differentiable bands and higher chemical specificity; 3) A Raman spectroscope collects spectra within seconds and enables real-time fast continuous scanning; and 4) non-contact and non-destructive analysis allows biological samples to be used for further examination. The innovative integration of SERS nanotag-labeled nanoplastics (model PS NPs) with the confocal SERS technique makes NPs traceable in biological samples.

After we synthesized the model PS NPs with SERS nanotags embedded using in-situ polymerization, we characterized the size and morphology using TEM. The TEM image clearly showed that the nAu cores were covered by a PS layer, creating a spherical core-shell structure (**Fig. 1a, 1b**). PS NPs (50 particles) were measured with ImageJ to determine the average size of the gold core and the thickness of the PS layer. The average nAu core diameter was 33.6 $\pm$ 0.65 nm. The PS shell thickness was 13.7 $\pm$ 0.18 nm, adding to 61.0 $\pm$ 0.66 nm (diameter) for the whole core-shell PS NP.

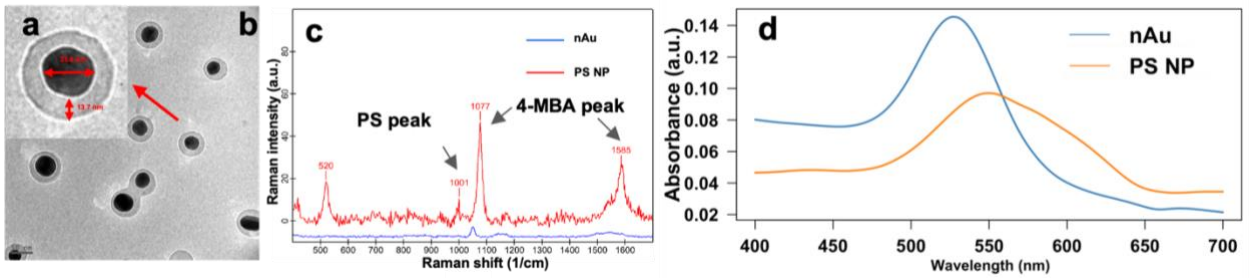

Fig. 1. Panels a-b are the TEM images of PS NPs, with panel a showing an enlarged image of one particle in core-shell structure. Panel c shows the comparison of Raman spectra between nAu (without tagging 4-MBA) and synthesized PS NPs. Panel d is the UV-Vis absorbance spectra of the synthesized PS NPs and nAu.

To examine if the nAu cores were labeled by the Raman indicator 4-MBA, we collected Raman spectra from both nAu and PS NPs. As observed in **Fig. 1c**, the model PS NPs displayed strong SERS signals (characteristic peaks of 4-MBA at 1077 cm^{-1} and 1585 cm^{-1}). Compared to the nAu cores (without tagging 4-MBA), the model PS NPs showed a distinct Raman spectrum pattern with significantly higher SERS signal intensity. In addition, the characteristic peak of PS is observed at 1001 cm^{-1} in the spectrum of model PS NPs, proving the successful formation of PS shell on nAu cores. However, the signal intensity at 1001 cm^{-1} is much lower than the peaks from the Raman indicator 4-MBA, suggesting that without using the Raman indicator 4-MBA, tracking PS NPs using the signal from PS itself would be challenging. Therefore, labeling the model NP cores with the Raman indicator 4-MBA is critical. Further, the UV-Vis spectra were recorded, which

underwent a redshift in the absorption maxima following the formation of PS on the nAu cores. (**Fig. 1d**). This shift can be attributed to both the increase in particle diameter and the presence of the PS coating.

3.2 Tap water washing

In this study, we first evaluated the tap water washing method for removing MNPs from basil leaves. To start with, we used PS MPs (42 µm) because they are observable under the Raman microscope due to their bigger size and strong Raman peaks even without any SERS tracers inside. Microscopic photos of PS MPs on a basil leaf before and after washing are shown in **Fig. 2a and 2e**, with the corresponding scanned areas marked in a red square. The Raman maps based on the characteristic peak of PS MPs (1001 cm^{-1}) showed a notable difference before and after washing with tap water. Raman signals of PS MPs were detectable before washing (**Fig. 2b**), but no signals were found afterward (**Fig. 2f**). The Raman map signals successfully matched the MPs observed in the microscopic images. To further demonstrate this, the overlaid images (**Fig. 2c, 2g**) confirmed that the signals correspond to PS MPs. The average Raman spectra of three replicates collected from the Raman maps are shown in **Fig. 2d**. The intensity of the PS characteristic Raman peak was notably higher before washing, but it significantly dropped after washing. This observation aligned with the Raman mapping results. The findings of all three replicates indicated that the tap water postharvest washing method was highly effective in removing PS MPs (42 µm). To compare each cleaning method in removing MNPs from basil leaves, the removal efficacies were calculated (**Fig. S7**) using the Removal Efficacy (RE) equation: RE = [(Raman intensity before washing -

Raman intensity after washing) / (Raman intensity before washing)] * 100%. The RE of the tap water washing method for removing PS MPs was calculated to be 93.1%.

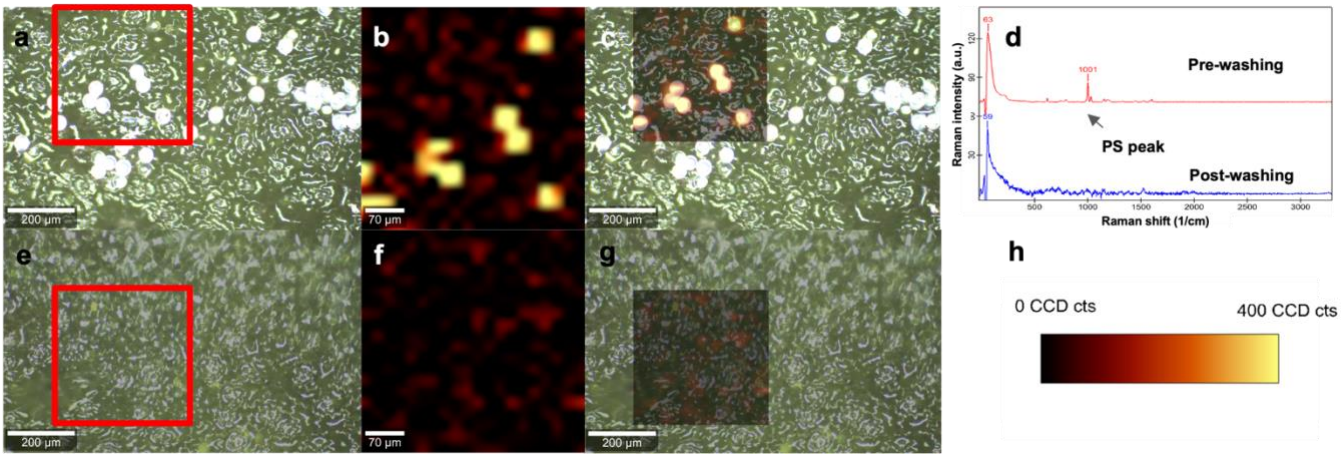

Fig. 2. Panels a-c show the microscopic image, Raman map scanned in the red square, and their overlaid image, respectively, for the sample with PS MPs (42 µm) on basil leaf before washing with tap water method. Panels e-g are the results for the same sample at the same scanned area after washing with the tap water method. The color scale bar of Raman mapping is shown in panel h. The average Raman spectra scanned on the leaf surfaces before and after washing with tap water method are shown in panel d. The characteristic peak of PS (1001 cm^{-1}) is marked with the arrow.

Subsequently, we applied the same washing method to assess its efficacy in removing smaller particles. Specifically, we focused on PMMA MPs with an average size of 6 µm. The scan area was randomly selected due to the uniform distribution of PMMA MP on the basil leaves as shown in **Fig. S2**. Based on the observation from the microscopic images (**Fig. 3a, 3e**), it was noted that a significant portion of the particles was removed, although a considerable number of PMMA MPs remained. The Raman maps also reflected this difference, with the post-washing map showing lower signals (**Fig. 3b, 3f**). Overlaid images were generated to visually represent the locations where signals were detected (**Fig. 3c, 3g**). The Raman spectra (**Fig. 3d**) demonstrated the partial removal of PMMA MPs from basil leaves by tap water washing with a RE of 51.6%, which aligned

with the visual observation from the microscopic images. To achieve more effective removal of small plastic particles, like 6 µm PMMA MPs, other postharvest washing methods are needed.

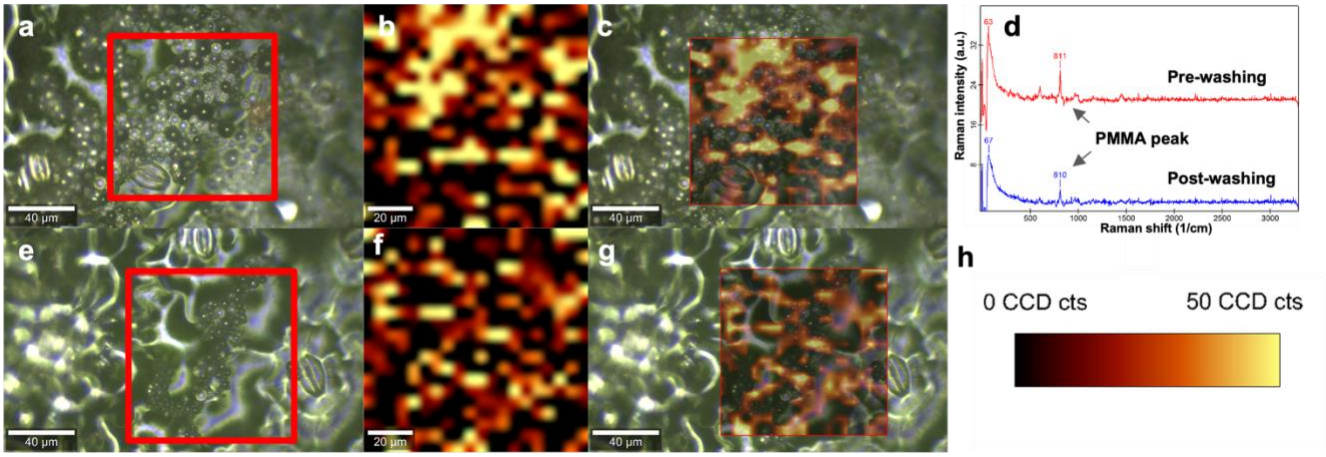

Fig. 3. Panels a-c show the microscopic image, Raman map scanned in the red square, and their overlaid image, respectively, for the sample with PMMA MPs (6 µm) on basil leaf before washing with tap water method. Panels e-g are the results for the same sample at the same scanned area after washing with the tap water method. The color scale bar of Raman mapping is shown in panel h. The average Raman spectra scanned on the leaf surfaces before and after washing with tap water method are shown in panel d. The characteristic peak of PMMA (811 cm^{-1}) is marked with the arrow.

The third type of plastic particles we assessed using tap water washing was the PS NPs (61 nm) synthesized above as the model NPs. Microscopic images were captured before and after washing in the same scanned area (**Fig. S5a, S5e**). However, because of their small size, individual particles of PS NP were not visible under the microscope. Considering the non-uniform distribution of PS NP droplets on the basil leaves (**Fig. S3**), to ensure an accurate assessment of the washing methods' efficacy, we chose to focus on the "coffee ring" during scanning. This area is the edge of the dried droplet where particles accumulate, enabling us to obtain the most distinct results for evaluating RE. Surprisingly, the Raman map showed stronger signals after washing the NP-contaminated leaf, with maximum intensity in one pixel reaching 200 CCD cts (**Fig. S5b, S5f**). To confirm that we scanned the identical area, we created an overlaid image (**Fig. S5c, S5g**), which verified our scanning accuracy. **Fig. S5d** showed the average SERS spectra of three replicates before and after washing. Consistently, all replicates demonstrated the same outcome: the average Raman intensity

increased in the scanned “coffee ring” area, indicating that the tap water washing method was ineffective in removing NPs from basil leaves. The increase in Raman intensity after washing was possibly attributed to the flushing action of tap water, which relocated some NPs to the “coffee ring”. This was tested through tap water washing of the PS NP on a smooth aluminum foil surface, and the same phenomenon occurred wherein the “coffee ring” area exhibited increased Raman signal intensity post-washing. (**Fig. S4**). The result suggested that the accumulation is mainly due to the “coffee ring” rather than the leaf surface structure.

The outcomes from the tap water washing method suggest its high efficacy in eliminating larger plastics such as 42 µm PS MPs. However, for smaller MNPs like 6 µm PMMA MPs and 61 nm PS NPs, the tap water washing method proved much less effective. The discovery underscores the significance of our study, revealing that tap water rinsing, as the most used household washing method, is insufficient for removing smaller-sized plastics. In the interest of food safety and public health, it is important to evaluate additional cleaning methods.

3.3 Vegetable detergent washing

Another common household cleaning method we chose to test is vegetable detergent for washing. This approach holds promise because it has the potential to change the surface properties of both plastics and basil leaves such as hydrophilicity, which might facilitate the following rinsing process with tap water. We specifically selected PMMA MPs and model NPs for this evaluation, considering their resistance to being removed by tap water rinsing alone.

The microscopic images captured before and after washing the PMMA MPs-contaminated leaf surface (**Fig. 4a, 4e**) clearly showed the effective removal of the particles. The Raman maps further confirmed a decrease in detected signals after the washing process (**Fig. 4b, 4f**). Averaged Raman spectra of three replicates (**Fig. 4d**) proved our hypothesis that soaking with vegetable detergent

followed by tap water rinsing was more effective in removing PMMA MPs than washing with tap water alone, with a RE of 73.3%.

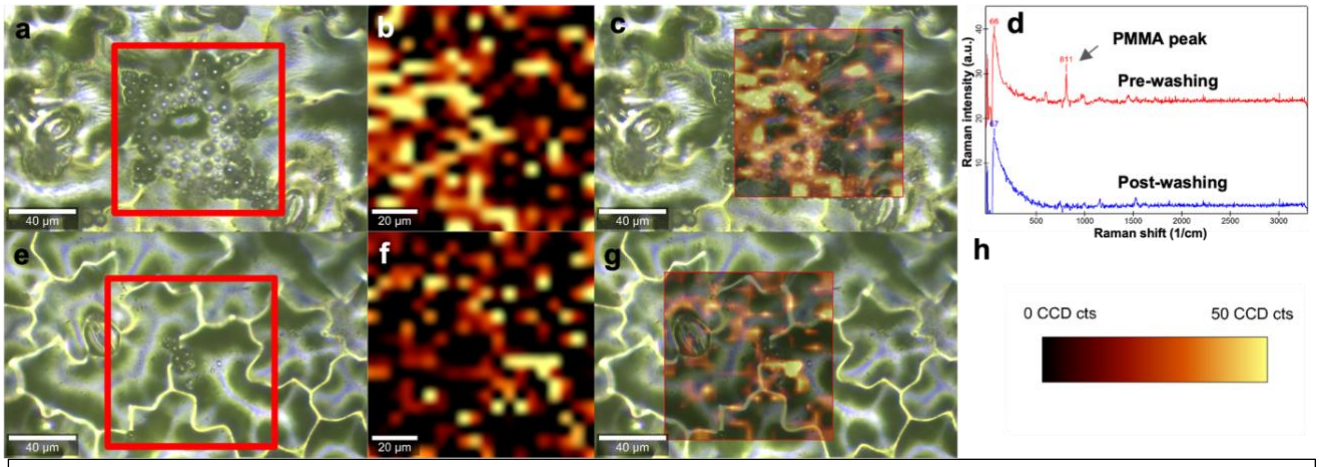

Fig. 4. Panels a-c show the microscopic image, Raman map scanned in the red square, and their overlaid image, respectively, for the sample with PMMA MPs (6 μm) on basil leaf before washing with vegetable detergent method. Panels e-g are the results for the same sample at the same scanned area after washing with the vegetable detergent method. The color scale bar of Raman mapping is shown in panel h. The average Raman spectra scanned on the leaf surfaces before and after washing with the vegetable detergent method are shown in panel d. The characteristic peak of PMMA (811 cm^{-1}) is marked with the arrow.

To assess the removal of PS NPs by vegetable detergent-assisted washing, the identical area was scanned before and after cleaning along the border of the "coffee ring" (**Fig. S6a, S6e)**. In **Fig. S6b**, the Raman map clearly shows the border of the dried PS NP droplet. However, after cleaning, the border became indistinct, and the shape of the droplet changed in **Fig. S6f**. Looking at the pixel colors in the Raman maps, it became obvious that the intensity increased, indicating a higher Raman intensity after cleaning. The overlaid images (**Fig. S6c, S6g**) once again confirmed the increase of PS NPs in the "coffee ring" after cleaning. To confirm this, we conducted three replicates, averaged the results, and generated Raman spectra, with results showing higher post-washing intensity compared to the pre-washing Raman intensity (**Fig. S6d**). This outcome parallels our findings from the tap water washing method, suggesting that the vegetable detergent cleaning method was ineffective in removing PS NPs from basil leaf and may relocate the PS NP particles to the "coffee ring" area (**Fig. S4**). The outcomes of this detergent cleaning method indicate its

capability to partially remove PMMA MPs from basil leaves, which had better efficacy than rinsing with tap water alone. However, for PS NPs, no removal was observed. Further cleaning strategies are still needed to address this challenge.

3.4 Sonication

We further assessed another cleaning method, sonication, to evaluate its efficacy in removing PMMA MPs and PS NPs from basil leaves. The hypothesis is that sonication could render the particles unstable on the basil leaf surface, facilitating their removal. The decrease in the amount of PMMA MPs post-washing was visible in the microscopic images. While a portion was removed, a considerable number of particles remained on the basil leaf surface after cleaning (**Fig. 5a, 5e**). The Raman maps and overlaid images visually indicated a reduction in the number of particles, as fewer pixels exhibited signals after the cleaning process (**Fig. 5b, 5c, 5f, 5g**). In addition, the Raman spectra revealed the Raman intensity of the PMMA characteristic peak before and after cleaning (**Fig. 5d**), with a removal efficacy of 22.6%. This shows the inadequacy of this cleaning method to eliminate PMMA MPs from the basil leaf surface.

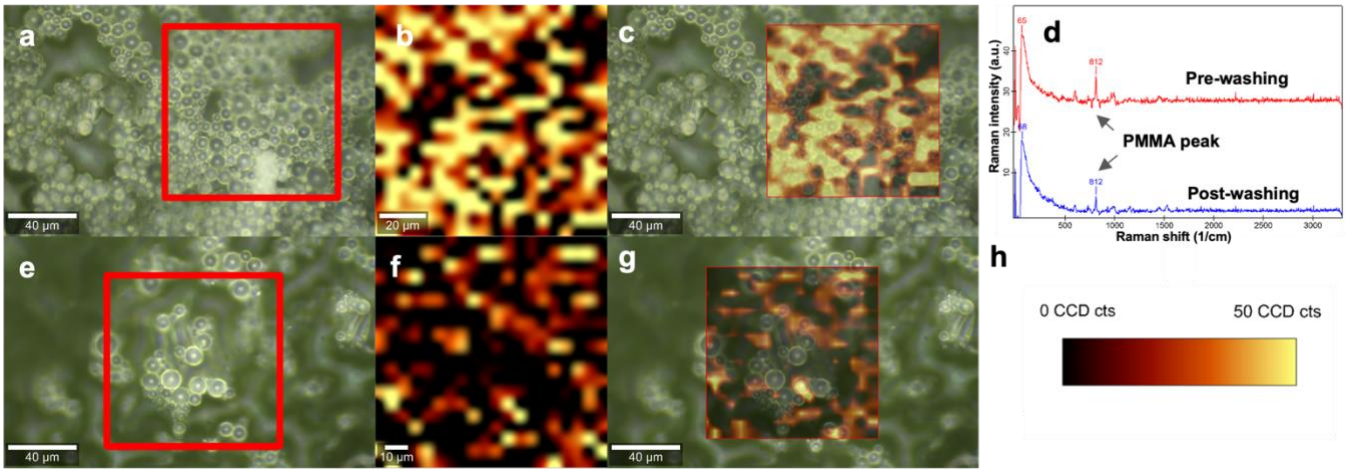

Fig. 5. Panels a-c show the microscopic image, Raman map scanned in the red square, and their overlaid image, respectively, for the sample with PMMA MPs (6 µm) on basil leaf before sonication. Panels e-g are the results for the same sample at the same scanned area after sonication. The color scale bar of Raman mapping is shown in panel h. The average Raman spectra scanned on the leaf surfaces before and after sonication are shown in panel d. The characteristic peak of PMMA (811 cm^{-1}) is marked with the arrow.

The same washing and detection protocol was applied to model PS NPs. The identical area was scanned by confocal Raman spectroscopy before and after sonication (**Fig. 6**). The average Raman spectra of the three replicates observed a slight reduction in intensity (**Fig. 6d**), with a removal efficacy of 11.1%, suggesting that sonication was better than the other two washing methods. However, in terms of effective removal, the sonication method is still insufficient.

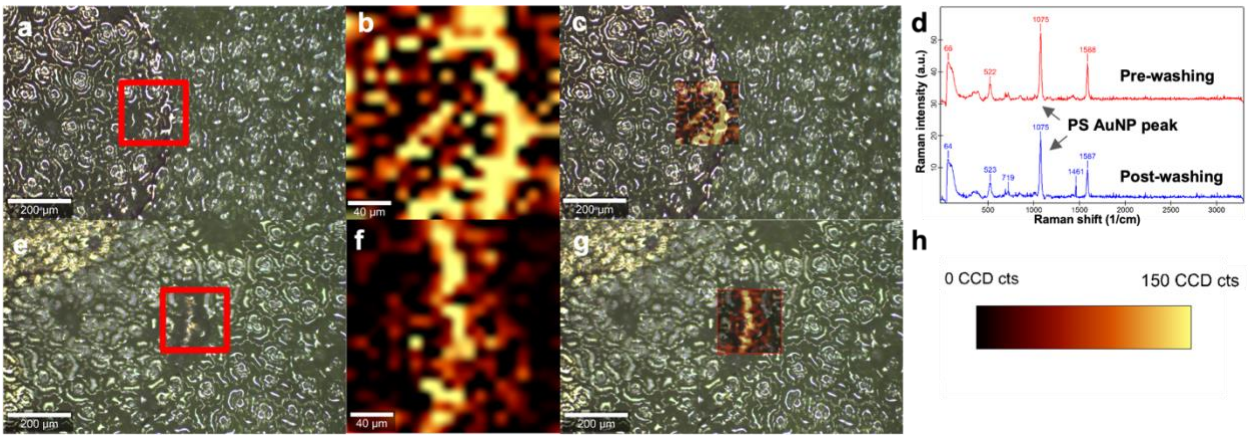

Fig. 6. Panels a-c show the microscopic image, Raman map scanned in the red square, and their overlaid image, respectively, for the sample with model NPs (61 nm) on basil leaf before sonication. Panels e-g are the results for the same sample at the same scanned area after sonication. The color scale bar of Raman mapping is shown in panel h. The average Raman spectra scanned on the leaf surfaces before and after sonication are shown in panel d. The characteristic peak of model PS NP (1078 cm^{-1}) is marked with the arrow.

3.5 model NP removal efficacy quantification by ICP-MS

Due to the results showing for the model NP removal, both the tap water washing method and detergent washing method exhibited negative removal efficacy. The hypothesis is that particles became trapped in the "coffee ring" of the droplet while washing. To gain a better understanding of the removal process, we used ICP-MS to quantify the difference in gold content on the entire basil leaves before and after washing, providing a more reliable measurement. As shown in **Fig. S7**, the removal efficacies of the tap water method and detergent method for removing model NP from bail leaves are relatively low, with removal efficacies of 16.46% and 16.85%, respectively.

These results are consistent with the findings from confocal Raman imaging. However, the removal efficacy of 59.8% for the sonication method demonstrated its effectiveness in removing model NP from basil leaves, which is also consistent with the confocal Raman imaging results. The ICP-MS quantification results further confirmed that the tap water and detergent washing methods are not effective enough to remove the model NP from basil leaves. These findings also support the hypothesis that the model NPs are relocated and trapped in the "coffee ring" during the washing process.

4. Conclusion

The results from three replicates consistently demonstrated that the tap water washing method was highly effective in eliminating PS MPs (42 μm) with an average removal efficacy of 93.1%. In contrast, the tap water washing method proved less effective in removing the 6 μm PMMA MP particles, with a RE of only 51.6%. These observations suggest that the RE is influenced by particle size and/or polymer type when using the tap water washing method. Among the three washing methods evaluated for PMMA MPs removal, the vegetable detergent method exhibited the highest RE, reaching up to 73.3%, while the sonication method only had a RE of 22.6%. Vegetable detergents containing surfactants can effectively lower the surface tension of water on vegetable leaves, facilitating the easier spreading of water over surfaces, and enabling water to lift surface contaminates and carry them away.[41] The method involved vegetable detergent soaking and a step of flushing with tap water, which enhanced the removal of PMMA particles from the basil leaves compared to flushing with tap water alone. To specifically examine the impact of particle size, we used the same polymer type, PS, but in a smaller size, PS NPs (61 nm) for evaluating the tap water washing method. The tap water washing method only exhibited a low removal efficacy of 16.5%. A similar phenomenon occurred with vegetable detergent washing for removing PS NPs. They

both suggest that tap water and vegetable detergent washing methods could relocate the PS NP particles, leading them to be trapped in the "coffee ring" (**Fig. S4**). Both methods failed to remove PS NPs from the basil leaf surfaces significantly while the sonication method exhibited the potential to partially remove PS NPs with a RE of 59.8%. This study provides valuable information and an approach to evaluate the RE of different washing methods in removing MNP contamination from fresh produce. The outcomes of this study underscore the need for the development of new and more effective decontamination techniques for MNP removal in the future.

Acknowledgments

We acknowledge the financial support from the SUNY Research Foundation startup fund [RF award 61476]. Research/Work reported in this work was also supported by the SUNY System Administration under the SUNY Research Seed Grant Award [Award# 95216].

Conflict of Interest

The authors declare no competing interests.

References

(1) Saeed, L.; Tohka, A.; Haapala, M.; Zevenhoven, R. Pyrolysis and Combustion of PVC, PVC-Wood and PVC-Coal Mixtures in a Two-Stage Fluidized Bed Process. *Fuel Processing Technology* **2004**, *85* (14), 1565–1583. https://doi.org/10.1016/J.FUPROC.2003.11.045.

(2) Sundqvist-Andberg, H.; Åkerman, M. Sustainability Governance and Contested Plastic Food Packaging – An Integrative Review. *J Clean Prod* **2021**, *306*, 127111. https://doi.org/10.1016/J.JCLEPRO.2021.127111.

(3) Klotz, M.; Haupt, M.; Hellweg, S. Potentials and Limits of Mechanical Plastic Recycling. *J Ind Ecol* **2023**, *27* (4), 1043–1059. https://doi.org/10.1111/jiec.13393.

(4) Choi, Y. R.; Kim, Y.-N.; Yoon, J.-H.; Dickinson, N.; Kim, K.-H. Plastic Contamination of Forest, Urban, and Agricultural Soils: A Case Study of Yeoju City in the Republic of Korea. https://doi.org/10.1007/s11368-020-02759-0/Published.

(5) Schwarz, A. E.; Ligthart, T. N.; Boukris, E.; van Harmelen, T. Sources, Transport, and Accumulation of Different Types of Plastic Litter in Aquatic Environments: A Review Study. *Mar Pollut Bull* **2019**, *143*, 92–100. https://doi.org/10.1016/J.MARPOLBUL.2019.04.029.

(6) Andrady, A. L. Microplastics in the Marine Environment. *Mar Pollut Bull* **2011**, *62* (8), 1596–1605. https://doi.org/10.1016/J.MARPOLBUL.2011.05.030.

(7) Andrady, A. L.; Barnes, P. W.; Bornman, J. F.; Gouin, T.; Madronich, S.; White, C. C.; Zepp, R. G.; Jansen, M. A. K. Oxidation and Fragmentation of Plastics in a Changing Environment; from UV-Radiation to Biological Degradation. *Science of The Total Environment* **2022**, *851*, 158022. https://doi.org/10.1016/J.SCITOTENV.2022.158022.

(8) Sun, J.; Wang, X.; Zheng, H.; Xiang, H.; Jiang, X.; Fan, J. Characterization of the Degradation Products of Biodegradable and Traditional Plastics on UV Irradiation and Mechanical Abrasion. *Science of The Total Environment* **2024**, *909*, 168618. https://doi.org/10.1016/J.SCITOTENV.2023.168618.

(9) Scholarship@western, S.; Cooper, D. A.; Corcoran, P. *Effects of Chemical and Mechanical Weathering Processes on the Degradation of Plastic Debris on Marine Beaches*; 2012. https://ir.lib.uwo.ca/etdhttps://ir.lib.uwo.ca/etd/371.

(10) Nguyen, L. H.; Nguyen, B. S.; Le, D. T.; Alomara, T. S.; AlMasoud, N.; Ghotekar, S.; Oza, R.; Raizada, P.; Singh, P.; Nguyen, V. H. A Concept for the Biotechnological Minimizing of Emerging Plastics, Micro- and Nano-Plastics Pollutants from the Environment: A Review. *Environ Res* **2023**, *216*, 114342. https://doi.org/10.1016/J.ENVRES.2022.114342.

(11) Emenike, E. C.; Okorie, C. J.; Ojeyemi, T.; Egbemhenghe, A.; Iwuozor, K. O.; Saliu, O. D.; Okoro, H. K.; Adeniyi, A. G. From Oceans to Dinner Plates: The Impact of Microplastics on Human Health. *Heliyon*. Elsevier Ltd October 1, 2023. https://doi.org/10.1016/j.heliyon.2023.e20440.

(12) Bank Editor, M. S. *Environmental Contamination Remediation and Management Microplastic in the Environment: Pattern and Process*. http://www.springer.com/series/15836.

(13) Horton, A. A.; Walton, A.; Spurgeon, D. J.; Lahive, E.; Svendsen, C. Microplastics in Freshwater and Terrestrial Environments: Evaluating the Current Understanding to Identify the Knowledge Gaps and Future Research Priorities. *Science of the Total Environment*. Elsevier B.V. May 15, 2017, pp 127–141. https://doi.org/10.1016/j.scitotenv.2017.01.190.

(14) Xia, W.; Rao, Q.; Deng, X.; Chen, J.; Xie, P. Rainfall Is a Significant Environmental Factor of Microplastic Pollution in Inland Waters. *Science of the Total Environment* **2020**, *732*. https://doi.org/10.1016/j.scitotenv.2020.139065.

(15) Hitchcock, J. N. Storm Events as Key Moments of Microplastic Contamination in Aquatic Ecosystems. *Science of The Total Environment* **2020**, *734*, 139436. https://doi.org/10.1016/J.SCITOTENV.2020.139436.

(16) O'Loughlin, J.; Finnan, J.; McDonnell, K. Accelerating Early Growth in Miscanthus with the Application of Plastic Mulch Film. *Biomass Bioenergy* **2017**, *100*, 52–61. https://doi.org/10.1016/J.BIOMBIOE.2017.03.003.

(17) van den Berg, P.; Huerta-Lwanga, E.; Corradini, F.; Geissen, V. Sewage Sludge Application as a Vehicle for Microplastics in Eastern Spanish Agricultural Soils. *Environmental Pollution* **2020**, *261*, 114198. https://doi.org/10.1016/J.ENVPOL.2020.114198.

(18) Ingman, M.; Santelmann, M. V.; Tilt, B. Agricultural Water Conservation in China: Plastic Mulch and Traditional Irrigation. *Ecosystem Health and Sustainability* **2015**, *1* (4), 1–11. https://doi.org/10.1890/EHS14-0018.1.

(19) Katsumi, N.; Kusube, T.; Nagao, S.; Okochi, H. The Input–Output Balance of Microplastics Derived from Coated Fertilizer in Paddy Fields and the Timing of Their Discharge during the Irrigation Season. *Chemosphere* **2021**, *279*, 130574. https://doi.org/10.1016/J.CHEMOSPHERE.2021.130574.

(20) Jiang, J. J.; Hanun, J. N.; Chen, K. Y.; Hassan, F.; Liu, K. T.; Hung, Y. H.; Chang, T. W. Current Levels and Composition Profiles of Microplastics in Irrigation Water. *Environmental Pollution* **2023**, *318*, 120858. https://doi.org/10.1016/J.ENVPOL.2022.120858.

(21) Oliveri Conti, G.; Ferrante, M.; Banni, M.; Favara, C.; Nicolosi, I.; Cristaldi, A.; Fiore, M.; Zuccarello, P. Micro- and Nano-Plastics in Edible Fruit and Vegetables. The First Diet Risks Assessment for the General Population. *Environ Res* **2020**, *187*, 109677. https://doi.org/10.1016/J.ENVRES.2020.109677.

(22) Lian, J.; Liu, W.; Meng, L.; Wu, J.; Chao, L.; Zeb, A.; Sun, Y. Foliar-Applied Polystyrene Nanoplastics (PSNPs) Reduce the Growth and Nutritional Quality of Lettuce (Lactuca Sativa L.). *Environmental Pollution* **2021**, *280*, 116978. https://doi.org/10.1016/J.ENVPOL.2021.116978.

(23) Dong, R.; Liu, R.; Xu, Y.; Liu, W.; Sun, Y. Effect of Foliar and Root Exposure to Polymethyl Methacrylate Microplastics on Biochemistry, Ultrastructure, and Arsenic Accumulation in Brassica Campestris L. *Environ Res* **2022**, *215*, 114402. https://doi.org/10.1016/J.ENVRES.2022.114402.

(24) Sun, H.; Lei, C.; Xu, J.; Li, R. Foliar Uptake and Leaf-to-Root Translocation of Nanoplastics with Different Coating Charge in Maize Plants. *J Hazard Mater* **2021**, *416*, 125854. https://doi.org/10.1016/J.JHAZMAT.2021.125854.

(25) Joardder, M. U. H.; Ananno, A. A.; Hossain, M. S. Food-Materials Cleaning: Current Trends and Recent Advances. *Postharvest and Postmortem Processing of Raw Food Materials: Unit Operations and Processing Equipment in the Food Industry* **2022**, 41–52. https://doi.org/10.1016/B978-0-12-818572-8.00003-6.

(26) Bilek, S. E.; Turantaş, F. Decontamination Efficiency of High Power Ultrasound in the Fruit and Vegetable Industry, a Review. *Int J Food Microbiol* **2013**, *166* (1), 155–162. https://doi.org/10.1016/J.IJFOODMICRO.2013.06.028.

(27) Kundu, A.; Shetti, N. P.; Basu, S.; Raghava Reddy, K.; Nadagouda, M. N.; Aminabhavi, T. M. Identification and Removal of Micro- and Nano-Plastics: Efficient and Cost-Effective Methods. *Chemical Engineering Journal* **2021**, *421*, 129816. https://doi.org/10.1016/J.CEJ.2021.129816.

(28) Walter, E. H. M.; Nascimento, M. da S. do; Kuaye, A. Y. Efficacy of Sodium Hypochlorite and Peracetic Acid in Sanitizing Green Coconuts. *Lett Appl Microbiol* **2009**, *49* (3), 366–371. https://doi.org/10.1111/j.1472-765X.2009.02670.x.

(29) Marfella, R.; Prattichizzo, F.; Sardu, C.; Fulgenzi, G.; Graciotti, L.; Spadoni, T.; D'Onofrio, N.; Scisciola, L.; La Grotta, R.; Frigé, C.; Pellegrini, V.; Municinò, M.; Siniscalchi, M.; Spinetti, F.; Vigliotti, G.; Vecchione, C.; Carrizzo, A.; Accarino, G.; Squillante, A.; Spaziano, G.; Mirra, D.; Esposito, R.; Altieri, S.; Falco, G.; Fenti, A.; Galoppo, S.; Canzano, S.; Sasso, F. C.; Matacchione, G.; Olivieri, F.; Ferraraccio, F.; Panarese, I.; Paolisso, P.; Barbato, E.; Lubritto, C.; Balestrieri, M. L.; Mauro, C.; Caballero, A. E.; Rajagopalan, S.; Ceriello, A.; D'Agostino, B.; Iovino, P.; Paolisso, G. Microplastics and Nanoplastics in Atheromas and Cardiovascular Events. *New England Journal of Medicine* **2024**, *390* (10), 900–910. https://doi.org/10.1056/nejmoa2309822.

(30) Zaheer, J.; Kim, H.; Ko, I. O.; Jo, E. K.; Choi, E. J.; Lee, H. J.; Shim, I.; Woo, H. jeong; Choi, J.; Kim, G. H.; Kim, J. S. Pre/Post-Natal Exposure to Microplastic as a Potential Risk Factor for Autism Spectrum Disorder. *Environ Int* **2022**, *161*, 107121. https://doi.org/10.1016/J.ENVINT.2022.107121.

(31) Zhu, Y. Y.; Ding, G. Q.; Ding, J. N.; Yuan, N. Y. AFM, SEM and TEM Studies on Porous Anodic Alumina. *Nanoscale Res Lett* **2010**, *5* (4), 725–734. https://doi.org/10.1007/s11671-010-9538-9.

(32) Liu, S.; Shang, E.; Liu, J.; Wang, Y.; Bolan, N.; Kirkham, M. B.; Li, Y. What Have We Known so Far for Fluorescence Staining and Quantification of Microplastics: A Tutorial Review. *Frontiers of Environmental Science and Engineering*. Higher Education Press Limited Company January 1, 2022. https://doi.org/10.1007/s11783-021-1442-2.

(33) Li, Z.; Feng, C.; Wu, Y.; Guo, X. Impacts of Nanoplastics on Bivalve: Fluorescence Tracing of Organ Accumulation, Oxidative Stress and Damage. *J Hazard Mater* **2020**, *392*, 122418. https://doi.org/10.1016/J.JHAZMAT.2020.122418.

(34) Catarino, A. I.; Frutos, A.; Henry, T. B. Use of Fluorescent-Labelled Nanoplastics (NPs) to Demonstrate NP Absorption Is Inconclusive without Adequate Controls. *Science of the Total Environment* **2019**, *670*, 915–920. https://doi.org/10.1016/j.scitotenv.2019.03.194.

(35) Schür, C.; Rist, S.; Baun, A.; Mayer, P.; Hartmann, N. B.; Wagner, M. When Fluorescence Is Not a Particle: The Tissue Translocation of Microplastics in Daphnia Magna Seems an Artifact. *Environ Toxicol Chem* **2019**, *38* (7), 1495–1503. https://doi.org/10.1002/etc.4436.

(36) Malafaia, G.; Luz, T. M. da; Ahmed, M. A. I.; Karthi, S.; Araújo, A. P. da C. When Toxicity of Plastic Particles Comes from Their Fluorescent Dye: A Preliminary Study Involving Neotropical Physalaemus Cuvieri Tadpoles and Polyethylene Microplastics. *Journal of Hazardous Materials Advances* **2022**, *6*, 100054. https://doi.org/10.1016/J.HAZADV.2022.100054.

(37) Eggeling, C.; Widengren, J.; Rigler, R.; Seidel, C. A. M. *Photobleaching of Fluorescent Dyes under Conditions Used for Single-Molecule Detection: Evidence of Two-Step Photolysis*; 1998.

(38) Li, Z.; Feng, C.; Wu, Y.; Guo, X. Impacts of Nanoplastics on Bivalve: Fluorescence Tracing of Organ Accumulation, Oxidative Stress and Damage. *J Hazard Mater* **2020**, *392*, 122418. https://doi.org/10.1016/J.JHAZMAT.2020.122418.

(39) Zhou, X. X.; He, S.; Gao, Y.; Chi, H. Y.; Wang, D. J.; Li, Z. C.; Yan, B. Quantitative Analysis of Polystyrene and Poly(Methyl Methacrylate) Nanoplastics in Tissues of Aquatic Animals. *Environ Sci Technol* **2021**, *55* (5), 3032–3040. https://doi.org/10.1021/acs.est.0c08374.

(40) Guo, H.; He, L.; Xing, B. Applications of Surface-Enhanced Raman Spectroscopy in the Analysis of Nanoparticles in the Environment. *Environmental Science: Nano*. Royal Society of Chemistry 2017, pp 2093–2107. https://doi.org/10.1039/c7en00653e.

(41) Kaushik, V.; Murudkar, S.; Gohil, K.; Ghatkar, S.; Gode, V.; Mhaskar, S. Review on Household Decontamination Technologies for Fruits & Vegetables. *International Journal of Food Science and Nutrition Engineering 2020* (1), 12–36. https://doi.org/10.5923/j.food.20201001.02.